ISSN 1990-7931, Russian Journal of Physical Chemistry B, 2016, Vol. 10, No. 6, pp. 935–945. © Pleiades Publishing, Ltd., 2016.
Original Russian Text © D.O. Glushkov, A.V. Zakharevich, P.A. Strizhak, S.V. Syrodoy, 2016, published in Khimicheskaya Fizika, 2016, Vol. 35, No. 11, pp. 14–25.

COMBUSTION, EXPLOSION, AND SHOCK WAVES

Effect of the Shape of an Organic Water–Coal Fuel Particle on the Condition and Characteristics of Its Ignition in a Hot Air Flow

D. O. Glushkov, A. V. Zakharevich, P. A. Strizhak*, and S. V. Syrodoy

Tomsk National Research Polytechnic University, Tomsk, 634034 Russia

**e-mail: pavelspa@tpu.ru*

Received October 26, 2015

Abstract—The results of experimental studies of the effect of the shape of an organic water–coal fuel (OCWF) particle on its ignition delay time and the time of its complete burnout in a hot air flow are reported. Three most common shapes of real particles, such as spherical, ellipsoidal, and irregular-polyhedron-like, are considered. It is shown that the shortest ignition delay time and the time of complete burnout correspond to polyhedron-shaped OCWF particles. Conditions are identified under which this factor significantly influences the ignition characteristics. The experiments were carried out at initial particle sizes (averaged maximum values) of 0.5–5 mm and temperatures and velocities of the oxidant flow of 600–900 K and 0.5–5 m/s, respectively. The main components of the studied fuels were coal processing wastes and waste motor, turbine, and transformer oils.

Keywords: organic water–coal fuel, water–coal slurry, coal processing waste, waste oils, hot air flow, ignition, combustion, ignition delay time, particle, shape

DOI: 10.1134/S199079311606004X

INTRODUCTION

The priority direction of development of engineering and technology "Energy efficiency, energy saving, and nuclear energy," as well as the critical technologies "Creation of efficient systems of transportation, distribution, and use of energy" and "Efficient production and conversion of energy from fossil fuels" [1] stress the importance of the issues of resource efficiency and energy saving in our country. This aspect motivates research and design work aimed at optimizing all stages of preparation and use of fuels for energy production. In the first place, it is advisable to effectively use fossil fuels (coal, oil, gas). It is worthwhile to mention a large group of works (see, e.g., [2–16]) on the development of new fuel compositions based on coals of different brands (including low-grade). Due to high environmental (and sometimes economic) indicators in comparison with solid fuels in their initial (coal-dust) state, coal–water fuels (CWF) and organic coal–water fuels (OCWF) or composite liquid fuels (CLF) are of considerable interest [7–12]. The latter can be composed [7–12] of coal dust, process or waste water, waste of coal and oil refining, waste oils, and other flammable liquids. At present, experimental data on the ignition of such fuels are scarce, being actually limited to those reported in [7–12]. As a consequence, the necessary conditions for the effective ignition and subsequent combustion of typical OCWF-based compositions remain insufficiently known.

The works [7–12] are devoted to studying the macroscopic characteristics of the combustion of OCWF at temperatures (typically below 1000 K) corresponding to the operation parameters of the boilers of modern power plants. An analysis of these works and the properties of the main components of OCWF suggests that, in order to optimize the cost of burning of such fuels in power plants, it is advisable to determine the limiting (necessary) conditions and relevant characteristics of sustainable ignition (in particular, low-temperature [17, 18], or limiting initiation of the combustion process at lowest possible temperatures sufficient for stable ignition). Low-temperature ignition [17, 18] is the initiation of the combustion of fuel at temperatures (600–800 K) significantly lower than those commonly used at power plants (typically above 1000 K). From the practical point of view, the main advantages of low-temperature ignition is the possibility to reduce the output of nitrogen and sulfur oxides and lower energy expenditures on the heating of the initiating its combustion.

The main purpose of the technologies of preparation and burning of OCWF is to effectively utilize typical waste of the chemical, petrochemical, coal, transportation, and other industries. Low-quality raw materials for OCWF accumulate annually in large

amounts. For example, only in Kuzbass, the stocks of low-grade coal and coal slurries exceed 20–30 million tons [19–21]. The volume of waste motor oil in the Siberian Federal District increases by a few hundred tons per year [19, 20]. Stocks of other possible OCWF components also constitute tens and even hundreds of tons in virtually every region of the country having the corresponding industries [19–21].

The determination of the conditions of low-temperature [17, 18] stable ignition of OCWF involves solving a group tasks, from analyzing the impact of each component on the ignition characteristics to finding the optimal values of the basic parameters of heat and mass transfer, phase transformations, and chemical reactions in the OCWF drop (particle)–oxidant. For example, it is useful to determine an optimal relationship between temperature and the oxidant flow rate and the size and shape of OCWF particles. In the first approximation, studies can be carried out for typical components OCWF such as filter cakes (FC), process water (or wastewater), and waste motor, turbine, and transformer oils. To analyze the effect of the oxidant parameters, temperature and speed, it is advisable to select somewhat wider ranges of their variation than those typical of the power industry: for example, 600–900 K and 0.5–5 m/s, respectively. This will set the conditions and integral characteristics of the low-temperature (or limiting) [17, 18] ignition of OCWF. However, the range of speeds of the oxidant flow should be limited to values at which fuel particles begin to be carried away by flow, which make it difficult to monitor the process. It is reasonable to select the sizes (diameters) of drops from those typical of standard power plant injectors (0.5 mm) to those at which the dispersion conditions are not realized (3–5 mm) [22–24]. The least studied (as can be judged by the works [25–27]) is the effect of the shape of particles (droplets) of composite fuels on the conditions of ignition in the oxidant flow.

It is interesting to examine how this factor influences the conditions of the low-temperature ignition of OCWF drops (particles). An analysis of the results obtained in [25–27] for typical OCWF shows that, most likely, it is appropriate to use the term "particle" instead of "drop," since the aggregate state of such fuels are generally pasty (jelly-like). In what follows, for the fuel compositions investigated, we will use the term "particle" instead of "drop."

The aim of the present work was to experimentally study how the shape of the OCWF particle influences the conditions and characteristics of its ignition in a heated air flow.

EXPERIMENTAL FACILITY AND PROCEDURES

The experiments were carried out on a setup schematically depicted in Fig. 1. In its main elements, it is similar to that used in [28–31]. The OCWF particle–oxidant flow system was considered (Fig. 1).

The main components of various OCWF compositions were offals (FC) of coal processing (Tables 1–3.) from the "Severnaya," "Kaltanskaya-Energeticheskaya," and "Chernigovskaya-Koksovaya" coal enrichment plants in the Kemerovo region. This approach made it possible to draw appropriate conclusions on the characteristics of the ignition of wastes of processing of solid fuels with significantly different properties [32–34]. All the FC had a jelly-like structure. These substances are a byproduct of coal beneficiation, whereby coal rock is washed with water containing surfactants. Water used for washing the rock is fed into special containers, where fine coal particles precipitate. Coal–water slurry is then pumped out and passed through press filters for water extraction. The moist residue (a mixture of water and coal) is known as filter coal. The average size of the coal dust particles in FC does not exceed 100 μm.

OCWF are prepared from liquid combustibles (Table 4), such as waste engine, turbine, and transformer oils. The components of different compositions were mixed for 10 min using a MPW-324 laboratory homogenizer.

The methodology of studying the integral characteristics of the ignition process included the following steps. An OCWF particle was heated in an air flow generated in quartz cylinder *1* with a length of 1 m and an internal diameter of 0.1 m (Fig. 1). The temperature T_g and speed V_g of the oxidant were varied within 600–900 K and 0.5–5.0 m/s, respectively, with blower *2* and heater *3*. The value of V_g was determined at an oxidant temperature of ~300 K using a UnionTest AN110 anemometer with a permissible systematic error of 0.05%. Preliminary experiments were carried out (assessments) at a flow rate above 10 m/s showed that OCWF particles are carried away from holder *4* (junction of low-inertia thermocouple) within a few milliseconds. Even the use of a high-speed video camera (10^5 frames/s) has not enabled to determine the ignition delay time, since the particle flew throughout a 1-m-long channel within a time tens times shorter (less than 0.1 s) than the ignition delay time. Such processes can only be studied in channels longer than 10 m, which are difficult to build in a laboratory. To record the ignition of moving particles, it would be necessary to use high-speed tracking systems and premises for their accommodation severalfold larger than the combustion camera (channel). In addition, the characterization of the ignition of a moving fuel particle involves large uncertainties in measuring the delay time, more specifically, it is difficult to identify conditions under which slow smoldering decay or intense heterogeneous combustion is realized.

Cylinder *1* (Fig. 1) had three technological holes located at the sidewall 0.4 m apart along the symmetry axis. The first and third holes, as countered in the

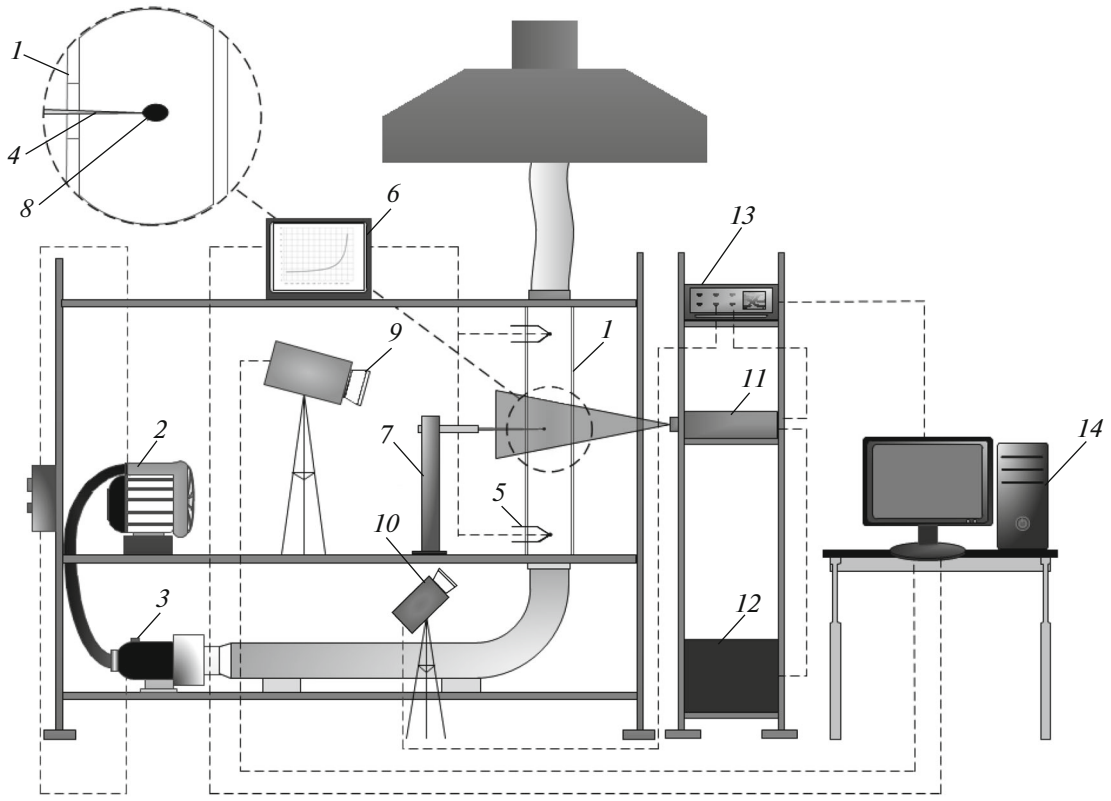

Fig. 1. Schematic diagram of the experimental setup: (*1*) hollow quartz glass cylinder, (*2*) blower, (*3*) heater, (*4*) low-inertia thermocouple, (*5*) thermocouple, (*6*) recorder, (*7*) coordinate mechanism (*8*) OCWF particle, (*9*) high-speed video camera, (*10*) cross-correlation camera, (*11*) two-pulse solid-state laser, (*12*) laser radiation generator, (*13*) synchronizer, and (*14*) personal computer.

direction of the air flow, were used to mount chromel-alumel thermocouples *5* (measuring within 273–1373 K with a systematic error of 3 K and a time constant of less than 10 s). Through the second hole, a 0.1-mm-diameter-junction platinum-rhodium–platinum thermocouple *4* (measuring within 273–1873 K to ±1 K with a time constant less than 1 s) was introduced into the cavity of cylinder *1* with coordinate mechanism *7* at a speed of 0.5 m/s. The signals from transducers *4* and *5* were fed into recorder *6* and used for monitoring the temperature T_d of fuel particle *8* the oxidant temperature in the respective sections of cylinder *1*.

OCWF particles were generated with a doser (with minimum and maximum volumes produced of 1 and 10 μL, respectively, and a dosing step of 0.1 μL). Using special dosing tips, particles of three shapes (spherical, ellipsoidal, and irregular polyhedron) under different operational modes (instantaneous flow rate, flow rate of supply of the composition, etc.) could be prepared. A particle was considered to be a irregular-shaped polyhedron if it had several (typically 5–7) well-pronounced vertices and faces. Before the experiment, the test particles were weighed using ViBRA HT 84RCE analytical balance.

A Phantom Miro M310 video cameras *9* (Fig. 1), with a filming speed of over 3000 frames/s and a full resolution of 1280 × 800 pixels) recorded the processes occurring during the induction period. Analyzing the

Table 1. Main characteristics of filter cakes (FC)

Sample	Mass fraction of dry coal, %	Q_s^a, MJ/kg
FC (wet) prepared from bituminous coal of grade "K," "Severnaya" coal enrichment plant, Kemerovo region	56.5	14.03
FC (wet) prepared from bituminous coal of grade "T," "Kaltanskaya-Energeticheskaya," Kemerovo region	60.9	16.4
FC (wet) prepared from bituminous coal of grade "SS," "Chernigovskaya-Koksovaya" coal enrichment plant Kemerovo region	62.1	9.46

Table 2. Results of technological analysis of FCs and coals

Sample	W^a, %	A^d, %	V^{daf}, %	Q_s^a, MJ/kg
FC (dry) prepared from bituminous coal of grade "K," "Severnaya" coal enrichment plant, Kemerovo region	–	26.46	23.08	24.83
Bituminous coal of grade "K," "Severnoe" coal field, Kemerovo region	2.05	14.65	27.03	29.76
FC (dry) prepared from bituminous coal of grade "T," "Kaltanskaya-Energeticheskaya," Kemerovo region	–	21.20	16.09	26.92
Bituminous coal of grade "T," "Kaltanskii" coal strip mine, Kemerovo region	2.89	18.07	15.07	27.65
FC (dry) prepared from bituminous coal of grade "SS," "Chernigovskaya-Koksovaya" coal enrichment plant, Kemerovo region	–	50.89	30.16	15.23
Bituminous coal of grade "SS," "Chernigovets" coal strip mine, Kemerovo region	2.76	21.68	27.40	26.23

Table 3. Results of elemental analysis of FCs and coals

Sample	C^{daf}, %	H^{daf}, %	N^{daf}, %	S^{daf}, %	O^{daf}, %
FC (dry) prepared from bituminous coal of grade "K," "Severnaya " coal enrichment plant, Kemerovo region	87.20	5.090	2.05	1.022	4.46
Bituminous coal of grade "K," "Severnoe" coal field, Kemerovo region	79.79	4.486	1.84	0.868	12.70
FC (dry) prepared from bituminous coal of grade "T," "Kaltanskaya-Energeticheskaya", Kemerovo region	90.13	4.255	2.31	0.441	2.77
Bituminous coal of grade "T," "Kaltanskii" coal strip mine, Kemerovo region	87.97	4.104	2.23	0.526	5.03
FC (dry) prepared from bituminous coal of grade "SS," "Chernigovskaya-Koksovaya" coal enrichment plant, Kemerovo region	87.47	5.039	2.15	0.444	4.77
Bituminous coal of grade "SS," "Chernigovets" coal strip mine, Kemerovo region	77.30	4.783	1.93	0.326	15.32

Table 4. Basic characteristics of waste oils

Sample	Density at 293 K, kg/m^3	Humidity, %	Ash content, %	Flash temperature, K	Ignition temperature, K	Heat of combustion, MJ/kg
Waste motor oil	871	0.28	0.78	405	491	44
Waste turbine oil	868	–	0.03	448	466	44.99
Waste transformer oil	877	–	–	421	442	44.98

data from recorder *6* and video camera *9* made it possible to determine the time evolution of the temperature T_d during the successive stages of the ignition of OCWF particles. The Tema Automotive specialized software [35, 36], incorporating an algorithm of continuous tracking of the videorecording area was used to determine the characteristic size of particles *8* and their position relative to the junction of low-inertia thermocouple *4*, as well as specific features of the ignition of fuel compositions. Processing of images to determine the particle size involved measuring four maximum sizes (irrespective of particle shape). For spherical particles, their diameters were determined. For ellipsoidal and polyhedron-shaped particles, axes

were drawn through the conventionally fixed center of mass at an angle of 45° (with a step relative to one another), and the maximum size of the particle was determined along each axis, after which algebraic averaging was performed. In this manner, the average values of the maximum sizes D_d of the particles were calculated. The initial sizes D_d ranged within 0.5–5.0 mm. The systematic error in determination of D_d at an appropriate resolution of high-speed videorecording did not exceed 4%. Controlling the process of enveloping the thermocouple junction with the OCWF film, with a permissible uncertainty in the film thickness is not more than 10% relative to the mean, makes it possible to reasonably claim that the centers of particle *8* and junction *4* coincide (Fig. 1). In the first approximation, the recorded data correspond to the temperature T_d at the center of the fuel composition particle. The systematic errors in determination of T_d and T_g for the channels comprised of thermocouples *4* and *5* and recorder *6*, were below 0.2 and 0.3%, respectively.

A time-lapse analysis of the videorecordings (at a rate of 1000 frames/s) of the processes under study enabled us to establish the instants of initiation and combustion termination, as well as the corresponding values of the ignition delay time t_d and the time of complete burnout t_c of the OCWF particle, counted from the moment particle *8* enter channel *1*. The systematic error in determination of t_d and t_c was 0.5×10^{-3} s. The events were identified according to a program in the image trigger mode. The tracking algorithm controlled the intensity (from 0 to 255) of shades of gray (from black to white) in the videorecording area. The combustion of the sample corresponded to an intensity range of 220–255. The moment of ignition is defined as the timing of first detection of a value from this range in any point located within the contour of the particle during the induction period. After combustion completion, the moment of decrease of the intensity at all points of the particle image to the value corresponding to the lower limit of the combustion range (less than 220) was fixed. An analysis of the data (values of t_d and t_c) and their comparison with the corresponding results on the change with time of the temperature of the particles (Fig. 2) made it possible to formulate criteria of initiation and termination of combustion. The ignition sets in when the following two conditions are met: the temperature of the particle exceeds the temperature the heating source (heated air flow, $T_d > T_g$) and the rate of change of particle temperature dT_d/dt exceeds 10 K/s. The end of the exothermic process is characterized by the reduction of the temperature of the solid residue to the temperature of the oxidant ($T_g \pm 0.05T_d^{max}$, where T_d^{max} is the maximum temperature of the particles during the combustion process).

To determine the specifics of the oxidant flow around the OCWF particle when its shape changes,

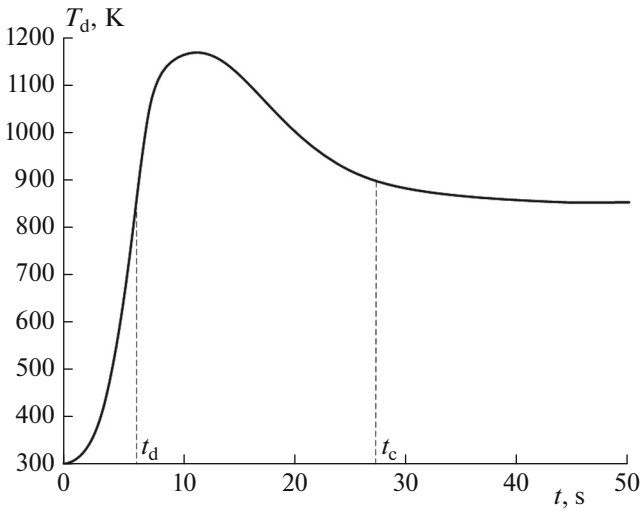

Fig. 2. Typical time evolution of the temperature of an ellipsoidal OCWF particle (95% FC (wet) prepared from bituminous coal of grade "K" + 5% waste motor oil) in the course of its interaction with the heating source at $T_g = 870$ K, $V_g = 5$ m/s, and $D_d = 3$ mm.

particle image velocimetry (PIV) experiments were performed [37–41]. For this, special tracers were introduced into the air flow. Similarly to the experiments carried out in [28–31], 80- to 100-nm titanium dioxide particles were added. During the movement in the cavity of cylinder *1*, the trajectory of the tracer particles corresponded to that of the air flow, which made it possible elucidate how the OCWF particle interacts with the heating source. To perform PIV measurements, cross-correlation camera *10* and two-pulse solid-state laser *11* were positioned near the particles, perpendicular to each other. The main elements of the cross-correlation videorecording system and the parameters of their operation were similar to those presented in [28–31]. The instantaneous field of oxidant flow velocity near the OCWF particle was measured by recording the movement of tracer particles within a fixed time interval. The measurement area of the dispersed flow was the laser knife plane dissecting the particle along its axis of symmetry. The tracer particles were repeatedly illuminated. Their images were recorded by the digital cross-correlation video camera. The subsequent processing of the images enabled to calculate the displacements of the tracer particles within the time between illuminations [37–41]. A detailed description of the method for calculating the velocity field of a gas flow with tracers is given in [30, 31]. According to the recommendations given in [30, 31], the concentration of tracer particles in the oxidant flow was 0.001–0.0012 m^3 per m^3 of gas. After refinement of the tracer velocity field near the OCWF particle, the main series of experiments on the ignition of OCWF particles (without adding tracer particles to the oxidant flow) were performed. In these experiments,

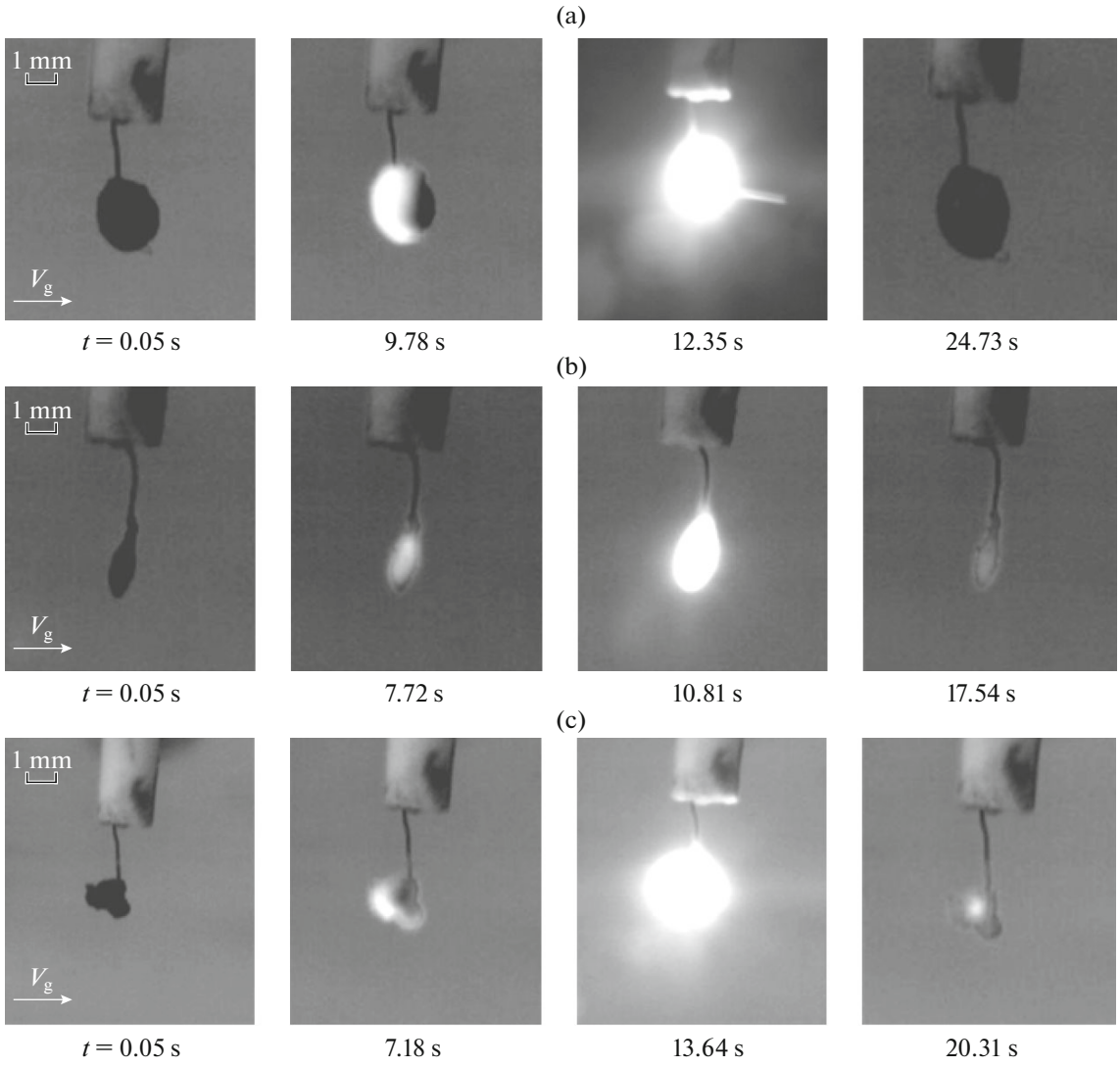

Fig. 3. Videorecordings of the heat-up, ignition, burning, and extinction of (a) spherical and (b) irregular-polyhedron-shaped OCWF particles (95% FC (wet) prepared from bituminous coal of grade "T" + 5% turbine waste oil) at $T_g \approx 870$ K and $V_g \approx 3$ m/s.

the cross-correlation videorecording elements were not used. The maximum systematic error in determining the oxidant velocity by PIV did not exceed 0.06 m/s (the elements of the cross-correlation instrumentation were tuned as described in [28–31]).

RESULTS AND DISCUSSION

Figure 3 shows typical images of a particle of one of the tested fuel compositions during its ignition and subsequent combustion in the oxidant flow. Observation by means of high-speed videorecording made it possible to identify the following stages of this process: reactionless heating of the OCWF particles; evaporation of moisture from its surface layer (accompanied by a reduction in its size and the change of the appearance of its surface from gloss to matt); intense evaporation of the liquid fuel component; transport of the thermal decomposition products of the coal organics; their heating, mixing, and intense gas-phase oxidation in the hot air; combustion of volatiles and evaporated flammable liquid; and heating and heterogeneous ignition of carbon and its burning to form an ash residue. The corresponding stages were identified according to the temperature T_d, which characterizes the absorption or release of energy in the fuel particle–air system.

The durations of the process seen in Fig. 3 for OCWF particles of different shapes make it possible to estimate the durations of the individual stages. These varied within 20–35% relative to the average values for the tested formulations (under identical conditions of heat transfer). However, the sequence of the stages persisted. This result enables to conclude that the overall mechanism of initiating the combustion of OCWF for different particle shapes and compositions

of the formulation in the above conditions of interaction with the oxidant flow.

The experiments with particles of different shapes (spherical, ellipsoidal, irregular polyhedron) have shown that the configuration of the surface produces a significant effect on the duration of almost all of the identified stages of the studied processes. In particular, the results presented in Fig. 4, obtained using the PIV method, illustrate the specifics of the oxidant flow around an OCWF particle.

For smooth-surface particles (spherical and ellipsoidal), the incoming flow separates occurred at the "equator" of the particle, which was accompanied by the formation of vortices behind the particle in the entire range of velocities V_g, from 0.5 to 5 m/s. In this zone, the air flow velocity (Fig. 4) was found to be substantially lower. For rough-surface particles (in particular, a polyhedron), the flow separation occurred near the frontal local zones of deceleration corresponding to the protrusions from the surface of the fuel particle. At the same time, local vortices arose near the rear side of the projections, with the subsequent formation of the main vortex behind the particle along the direction of the flow. The established specifics of the interaction of particles of different shapes with a hot air flow makes it possible to analyze the impact of this factor on the characteristics of the ignition of OCWF particles, such as the location of the combustion zone (if any) of the gas mixture (vapors, volatiles, and oxidant), the zone of ignition of the carbonaceous residue of the particle, and the delay time of ignition of the latter.

Heating the OCWF particle initiated the evaporation and thermal decomposition of its solid and liquid components. These two processes occurred more intensely on the frontal side of the particle and less intensely, on the rear side, in the region of lower air flow rates (Fig. 4). The vapor and volatiles released were partially carried away by the flow, with the maximum concentration of combustible gas mixture being achieved in the area of formation of vortices near the rear side of the particle. In some experiments, a gas mixture flame was observed in this area.

Because of the evaporation of moisture and release of volatiles, in a small area on the frontal surface of the particle, the conditions for the ignition of the carbonaceous residue were achieved (Fig. 3). The combustion front propagated over the surface of the particle in the direction of movement of the air flow. The conditions for the propagation of the combustion front and burnout of the carbon residue were identical for the particles of different shapes, in contrast to the initial stage of the process.

Irregularly shaped particles are characterized by shorter ignition delay times (Fig. 5). This result can be explained by a more intense heating of the individual projections of rough-surface particles. In contrast to particles with smooth surface, such protrusions facilitate the process of ignition. The duration of the heat-

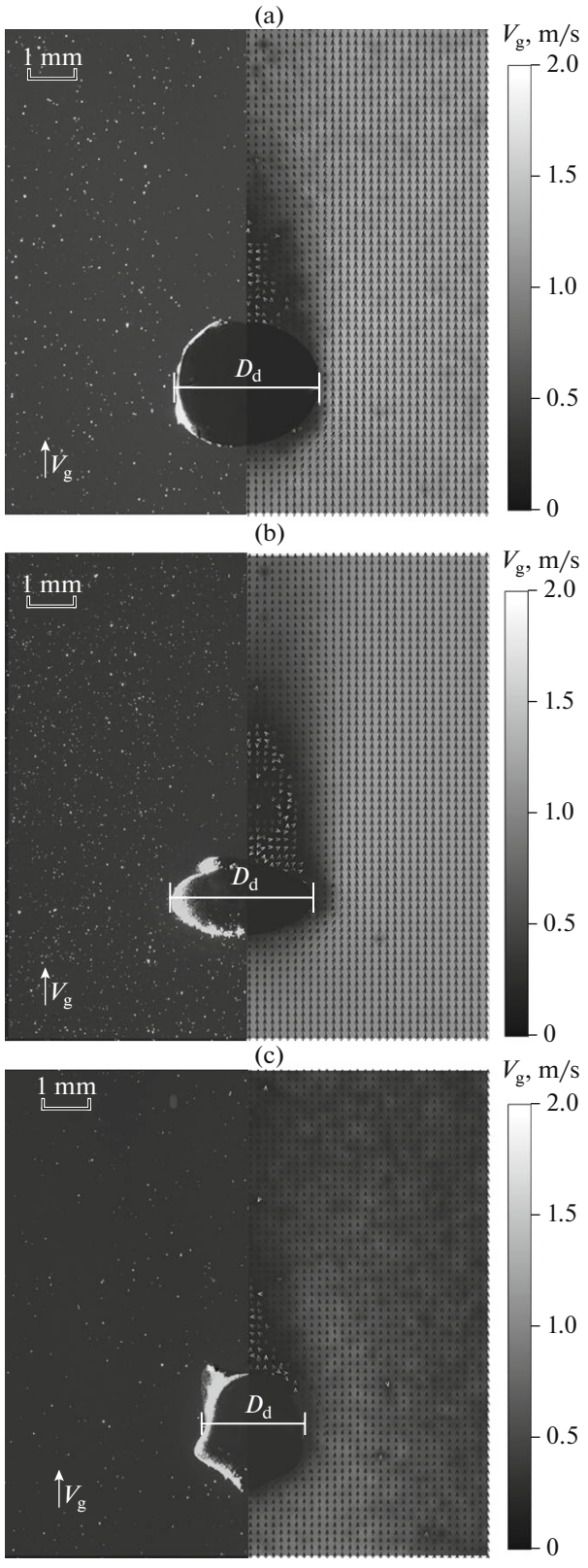

Fig. 4. Image of (a) spherical, (b) ellipsoidal and (c) irregular-polyhedron-shaped OCWF particles (95% FC (wet) prepared from bituminous coal of grade "K" + 5% waste transformer oil) (left) and the air flow velocity distribution (right) nearby.

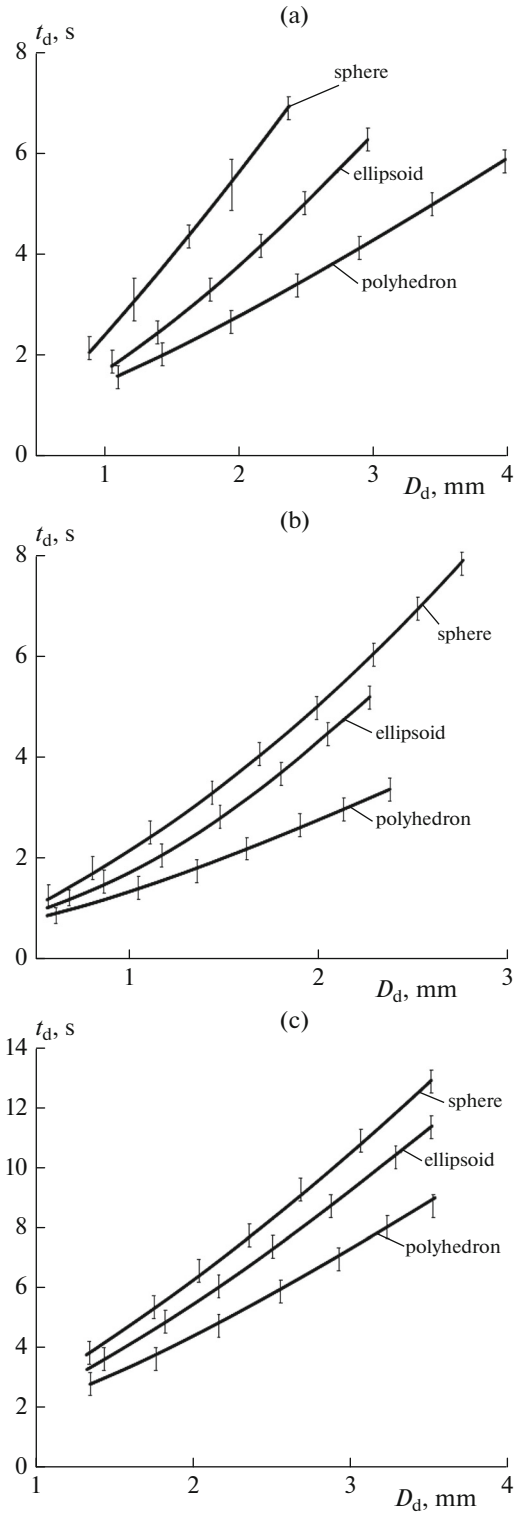

Fig. 5. Dependences of the ignition delay time on the initial size of OCWF particles of the following compositions: (a) 95% FC (wet) prepared from bituminous coal of grade "K" + 5% waste motor oil; (b) 95% FC (wet) prepared from bituminous coal of grade "T" + 5% waste motor oil; and (c) 95% FC (wet) prepared from bituminous coal of grade "SS" + 5% waste motor oil. $T_g \approx 870$ K, $V_g \approx 5$ m/s.

up of an individual projection until the carbonaceous residue is ignited is significantly shorter than the duration of the induction period before the formation of local zones of ignition of spherical and ellipsoidal particles. This result can be explained by the fact that, for such particles, in contrast to rough-surface particles, characterized by an intense heat flux from the heating zone of the near-surface layer into the bulk of the particle, which leads to an increase in the duration of the reactionless heating stage.

With increasing size of the OCWF particle, the above effects its shape on the ignition characteristics become more pronounced. This is due to an increase in the aerodynamic forces acting on the particle, a rise in the mass flux of flammable liquid vapors and thermal decomposition products from its surface, and an increase the rate of their chemical interaction with the oxidant flow.

It is found that, large-size particles, combustion can be initiated at lower temperatures of the heat source as compared to small particles (e.g., for 1.5-mm particles, the minimum temperature required for their ignition is by 70–90 K lower than that needed for 0.5-mm particles). Along with this, under identical heating conditions, small particles ignite more quickly (with a shorter delay) as compared to larger particles (Fig. 5). An analysis of videorecordings of the experiments performed suggests that this is due to the peculiarities of the formation of local ignition zones in the near-surface layer of small particles. With increasing size D_d increases the mass flux from the surface of thermal decomposition products and vapors of liquid components. This increases the concentration of combustible gases in the near-surface layer of the OCWF particle. Particles with small D_d are characterized by shorter reaction less heat-up inert times. However, the concentration of flammable gases released from small particles is insufficient for sustained ignition. In experiments with particles with $D_d \le 0.5$ mm, local ignition hotspots are formed in the initial stage of heating without initiation of the stable combustion of OCWF. Videorecordings of the process have shown that volatiles and vapors of combustible and incombustible liquids are entrained by the oxidant flow more rapidly than in the case of large particles. These processes hamper the ignition of fine OCWF particles at relatively low temperatures, at which large particles are ignited.

It was also found that the effect of particle shape on the ignition characteristics of OCWF might be pronounced or rather moderate, depending on the composition of the fuel (Fig. 5). The experiments performed have shown that this feature is due to the influence of the properties of the corresponding coal components of the OCWF (Tables 1–4) at the stage of ignition: FC of brand "K" is characterized by a fairly similar humidity, small ash content, and the highest content of volatiles as compared to brands "T" and "SS"; the content of volatiles is a decisive factor in ini-

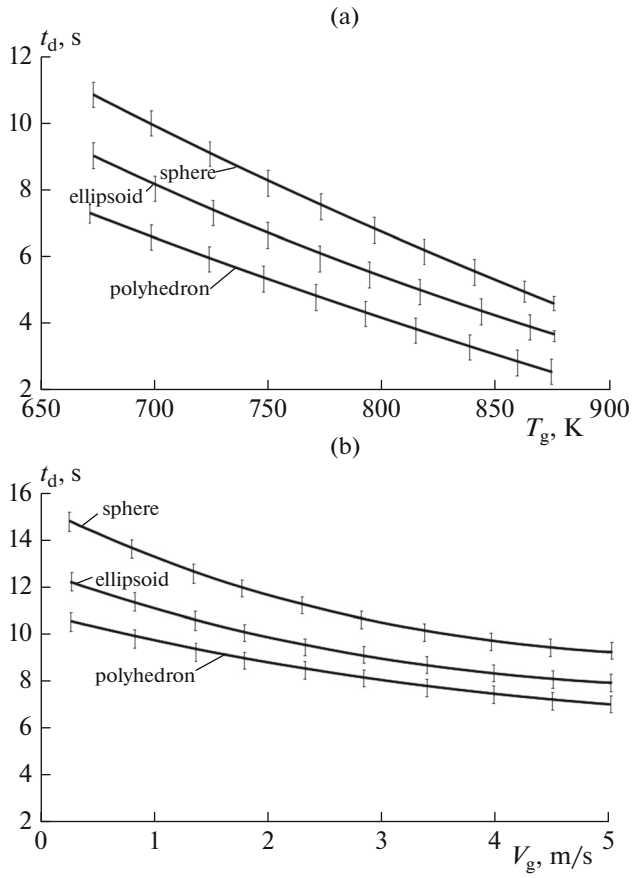

Fig. 6. Dependences of the ignition delay time of an OCWF particle (95% FC (wet) prepared from bituminous coal of grade "K" + 5% waste motor oil) on the (a) temperature at $V_g \approx 5$ m/s and (b) air flow velocity at $T_g \approx 670$ K; $D_d = 1.5$ mm in both cases.

tiating the process of combustion. In particular, when using FC produced from bituminous coal of grade "K," the influence of the particle shape is quite significant (in Fig. 5a; variations in the time t_d reach 30% for the considered shapes). For compositions based on FC prepared from bituminous coal of grades "T" and "SS," such variations do not exceed 10–15%.

The $t_d = f(T_g)$ dependences in Fig. 6 show that, with increasing temperature of the oxidant and increasing heat transfer intensity, the effect of particle shape on the integral characteristics of the ignition of OCWF diminishes. This result suggests that, for OCWF to be applicable in the power industry, it is advisable to use specialized sieves and devices for modifying the surface of the particles (imparting them shapes of irregular polyhedra) so as to make them burn at the lowest (in sustainable ignition range) possible temperature, or ignite them at higher temperatures (e.g., 900–1200 K), at which the role of the shape factor is insignificant.

For the dependence displayed in Figs. 5 and 6, the following approximation expressions were obtained:

—for a composition containing 95% FC of brand "K" + 5% waste motor oil

$$t_d = 2.3 D_d^{1.26},\ 1 \le D_d \le 2.5 \text{ mm (sphere)},\ T_g \approx 870 \text{ K},\ V_g \approx 5 \text{ m/s};$$

$$t_d = 1.81 D_d^{1.41},\ 1 \le D_d \le 3 \text{ mm (ellipsoid)},\ T_g \approx 870 \text{ K},\ V_g \approx 5 \text{ m/s};$$

$$t_d = 1.39 D_d^{1.07},\ 1 \le D_d \le 4 \text{ mm (polyhedron)},\ T_g \approx 870 \text{ K},\ V_g \approx 5 \text{ m/s};$$

—for a composition containing 95% FC of brand "T" + 5% waste motor oil

$$t_d = 2.21 D_d^{1.37},\ 0.5 \le D_d \le 3 \text{ mm (sphere)},\ T_g \approx 870 \text{ K},\ V_g \approx 5 \text{ m/s};$$

$$t_d = 1.89 D_d^{1.33},\ 0.5 \le D_d \le 2.3 \text{ mm (ellipsoid)},\ T_g \approx 870 \text{ K},\ V_g \approx 5 \text{ m/s};$$

$$t_d = 1.59 D_d^{0.96},\ 0.5 \le D_d \le 2.5 \text{ mm (polyhedron)},\ T_g \approx 870 \text{ K},\ V_g \approx 5 \text{ m/s};$$

—for a composition containing 95% FC of brand "SS" + 5% waste motor oil

$$t_d = 2.97 D_d^{1.15},\ 0.5 \le D_d \le 3.5 \text{ mm (sphere)},\ T_g \approx 870 \text{ K},\ V_g \approx 5 \text{ m/s};$$

$$t_d = 2.61 D_d^{1.15},\ 0.5 \le D_d \le 3.5 \text{ mm (ellipsoid)},\ T_g \approx 870 \text{ K},\ V_g \approx 5 \text{ m/s};$$

$$t_d = 2.04 D_d^{1.16},\ 0.5 \le D_d \le 3.5 \text{ mm (polyhedron)},\ T_g \approx 870 \text{ K},\ V_g \approx 5 \text{ m/s};$$

—for a composition containing 95% FC of brand "K" + 5% waste motor oil

$$t_d = 5 \cdot 10^{10} T_g^{-3.43},\ 670 \le T_g \le 870 \text{ K (sphere)},\ D_d \approx 1.5 \text{ mm},\ V_g \approx 5 \text{ m/s};$$

$$t_d = 5 \cdot 10^{11} T_g^{-3.81},\ 670 \le T_g \le 870 \text{ K (ellipsoid)},\ D_d \approx 1.5 \text{ mm},\ V_g \approx 5 \text{ m/s};$$

$$t_d = 3 \cdot 10^{12} T_g^{-4.12},\ 670 \le T_g \le 870 \text{ K (a polyhedron)}\ D_d \approx 1.5 \text{ mm},\ V_g \approx 5 \text{ m/s};$$

$$t_d = 5.29 V_g^{-0.09},\ 0.5 \le V_g \le 5 \text{ m/s},\ D_d \approx 1.5 \text{ mm (sphere)},\ T_g \approx 670 \text{ K};$$

$$t_d = 4.15 V_g^{-0.13},\ 0.5 \le V_g \le 5 \text{ m/s},\ D_d \approx 1.5 \text{ mm (ellipsoid)},\ T_g \approx 670 \text{ K};$$

$$t_d = 2.9 V_g^{-0.12},\ 0.5 \le V_g \le 5 \text{ m/s},\ D_d \approx 1.5 \text{ mm (polyhedron)},\ T_g \approx 670 \text{ K}.$$

The dependencies of the ignition delay time on of the three main parameters of the processes (T_g, V_g, and D_d) suggest the oxidant flow rate is the least influential factor. This result is important, since it demonstrates

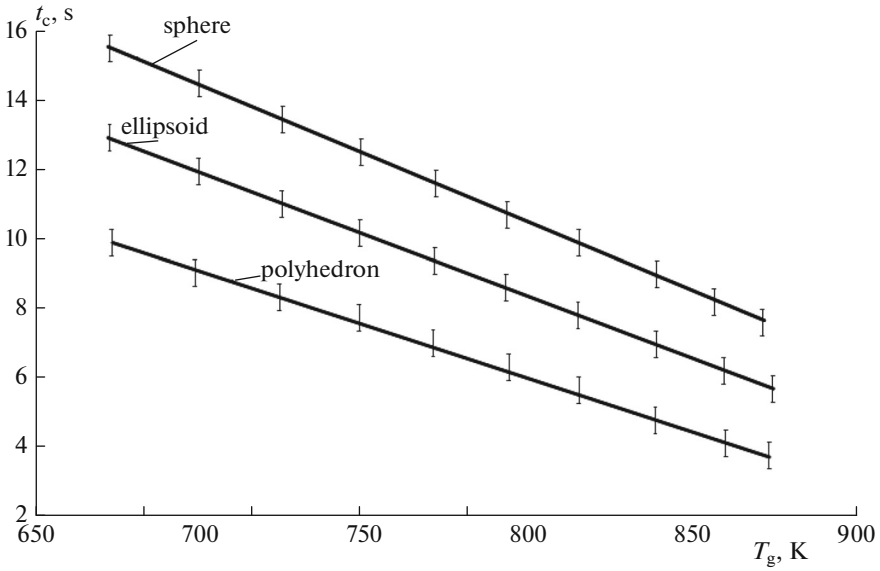

Fig. 7. Time of complete burnout of OCWF particles (FC 95% (wet) prepared from bituminous coal of grade "K" + 5% waste motor oil) on the air flow temperature at $V_g \approx 5$ m/s and $D_d = 1.5$ mm.

the possibility of fairly substantially optimization of OCWF combustion technologies (due to lower expenditures on the formation of the oxidant flow and its acceleration). That the effect of V_g is smaller is due to the relevant specific feature of the influence of convective and radiative heat fluxes at the fuel particle–oxidant interface. Theoretical evaluations based on the expressions $q_c = \alpha(T_g - T_s)$ and $q_r = \varepsilon\sigma(T_g^4 - T_s^4)$ show that at $T_g = 650$ K, values of q_r may exceed q_c nearly 1.3- to 1.5-fold. With increasing T_g, the difference between q_r and q_c grows nonlinearly. In particular, at $T_g = 900$ K, q_r is greater than q_c by a factor of 2–3.

The above estimates of the influence of the shape of the particle on the conditions and characteristics of its ignition enabled us to establish their close correlation with the aerodynamic drag coefficient k_g for the corresponding configurations [42–44]. In particular, the values of this parameter [42–44] were found to be 0.47 for a sphere, 0.53 for an ellipsoid, and 0.83 for an irregular polyhedron. For example, for the low temperature ignition of an OCWF containing waste motor oil (at an oxidant temperature of 650–800 K), the differences t_d values of t_d for spherical and ellipsoidal particles constitute on average 10–14%. The values of k_g for these shapes differ by almost 13%. The values of k_g for irregular-polyhedron-shaped and spherical particles may vary by 35–45%. Experiments with thus shaped OCWF particles showed that the values of t_d at $T_g = 800$–900 K, for example, for these configurations differ by 30–40%. At lower values of T_g, the difference reached 60%. These features illustrate how the ignition delay time of OCWF particles of different shapes can be predicted in a simple way by using the respective values of k_g and known values of t_d for one of the shapes. Note, however, that this approach can be used only at $T_g < 800$ K, since in this case the duration of the reactionless heat-up of the OCWF particle constitutes a large fraction of t_d (about half). With increasing T_g, this effect becomes less important, so that the time t_d can be evaluated based on known k_g only with a rather large uncertainty.

The temperature dependences displayed in Fig. 7 demonstrate the decisive contribution of the ignition delay time (Fig. 6a) to the time of complete burnout (t_c) of OCWF particles. It is rather clearly seen that the time t_d determines the monotony of the relevant dependences of the time t_c. The experiments showed that, at oxidant temperatures above 800 K, the duration of the reactionless heat-up of the particles before the active stage of its ignition is comparable to the total time of combustion. Therefore, the contribution of t_d to t_c turns out to be somewhat reduced. At lower temperatures, the value of t_d constitutes 50–75% of the time t_c. This shows the paramount importance of the individual stages of the ignition of OCWF ignition in studying of their combustion.

CONCLUSIONS

(1) The ignition delay times for irregular-polyhedra-shaped particles are shorter as compared to spherical and ellipsoidal particles.

(2) The effect of shape of the OCWF particle on its integrated ignition characteristics is significant at $T_g <$ 800 K and $D_d < 3$ mm.

(3) The shape of the OCWF particle may substantially affect not only the times t_d and t_c, but also the ignition mechanism. In particular, irregular-polyhedron-shaped particles are prone to disintegration, followed by the ignition of detached OCWF fragments.

(4) To minimize the expenditures on the burning of OCWF in power plants, it is advisable to use specialized devices (e.g., sieves or gratings) for preparing irregular-polyhedra-shaped particles.

(5) The effects observed extend the current understanding of the process of OCWF ignition. These effects can be used in developing appropriate models of heat and mass transfer in the conditions of phase transitions and chemical reactions.

ACKNOWLEDGMENTS

This work was supported by the Russian Science Foundation, project no. 15-19-10003.

REFERENCES

1. Presidential Decree number 899 of July 7, 2011, On approval of the priority directions of science, technology, and engineering development in the Russian Federation and the list of critical technologies of the Russian Federation; http://www.kremlin.ru/acts/bank/33514
2. P. A. Shchinnikov, E. A. Yevtushenko, Yu. V. Ovchinnikov, et al., Therm. Eng., No. 7, 30 (2001).
3. E. G. Gorlov, Khim. Tverd. Topl., No. 6, 50 (2004).
4. G. S. Khodakov, E. G. Gorlov, and G. S. Golovin, Khim. Tverd. Topl., No. 6, 15 (2005).
5. G. S. Khodakov, E. G. Gorlov, and G. S. Golovin, Khim. Tverd. Topl., No. 4, 22 (2006).
6. A. I. Borzov and M. P. Baranova, Khim. Tverd. Topl., No. 4, 40 (2006).
7. G. S. Khodakov, Therm. Eng. **54**, 36 (2010).
8. E. G. Gorlov, A. I. Seregin, and G. S. Khodakov, Solid Fuel Chem. **41**, 364 (2007).
9. K. N. Trubetskoi, V. E. Zaidenvarg, A. C. Kondrat'ev, V. I. Murko, G. A. Kassikhin, and I. Kh. Nekhoroshii, Therm. Eng. **45**, 413 (2010).
10. E. G. Gorlov, A. I. Seregin, and G. S. Khodakov, Solid Fuel Chem. **42**, 208 (2008).
11. I. I. Lishtvan, P. L. Falyushin, E. A. Smolyachkova, and S. I. Kovrik, Solid Fuel Chem. **43**, 1 (2009).
12. A. I. Tsepenok, Yu. V. Ovchinnikov, Yu. V. Strizhko, and S. V. Lutsenko, Energetik, No. 7, 45 (2011).
13. A. Kijo-Kleczkowska, Fuel **90**, 865 (2011).
14. N. I. Red'kina, G. S. Khodakov, and E. G. Gorlov, Solid Fuel Chem. **47**, 306 (2013).
15. A. P. Burdukov, V. I. Popov, M. Y. Chernetskiy, A. A. Dekterev, and K. Hanjalić, Appl. Therm. Eng. **74**, 174 (2015).
16. S. Belošević, I. Tomanović, V. Beljanski, D. Tucaković, and T. Živanović, Appl. Therm. Eng. **74**, 102 (2015).
17. D. O. Glushkov, G. V. Kuznetsov, and P. A. Strizhak, Solid Fuel Chem. **49**, 73 (2015).
18. D. O. Glushkov, G. V. Kuznetsov, and P. A. Strizhak, Russ. J. Phys. Chem. B **9**, 242 (2015).
19. Yu. F. Patrakov, N. I. Fedorova, and A. I. Efremov, Vestn. Kuzbas. Tekh. Univ., No. 2, 81 (2006).
20. Yu. V. Ovchinnikov, A. I. Tsepenok, A. V. Shikhotinov, and E. V. Tatarnikova, Dokl. Akad. Nauk Vyssh. Shkoly RF, No. 1, 117 (2011).
21. V. A. Arkhipov, A. M. Sidor, and V. G. Surkov, Tekh. Teplofiz. Prom-sti Teploenerget., No. 5, 39 (2013).
22. L.-P. Hsiang and G. M. Faeth, Int. J. Multiphase Flow **19**, 721 (1993).
23. E. H. Trinh, R. G. Holt, and D. B. Thiessen, Phys. Fluids **8**, 43 (1996).
24. A. K. Flock, D. R. Guildenbecher, J. Chen, P. E. Sojka, and H.-J. Bauer, Int. J. Multiphase Flow **47**, 37 (2012).
25. W. Gajewski, A. Kijo-Kleczkowska, and J. Leszczynski, Fuel **88**, 221 (2009).
26. J. Zhu, G. Zhang, G. Liu, Q. Qu, and Y. Li, Fuel Proc. Technol. **118**, 187 (2014).
27. L. Bartoňová, Fuel Proc. Technol. **134**, 136 (2015).
28. R. S. Volkov, G. V. Kuznetsov, and P. A. Strizhak, Int. J. Heat Mass Transfer **79**, 838 (2014).
29. D. O. Glushkov, D. P. Shabardin, P. A. Strizhak, and K. Yu. Vershinina, Fuel Proc. Technol. **143**, 60 (2016).
30. D. O. Glushkov, P. A. Strizhak, and K. Yu. Vershinina, Appl. Therm. Eng. **96**, 534 (2016).
31. R. S. Volkov, G. V. Kuznetsov, and P. A. Strizhak, Int. J. Therm. Sci. **88**, 193 (2015).
32. B. V. Novozhilov, *Non-Stationary Combustion of Solid Rocket Fuels* (Nauka, Moscow, 1973) [in Russian].
33. L. K. Gusachenko, V. E. Zarko, V. Ya. Zar'yanov, and V. P. Bobryshev, *Simulation of Solid Fuel Combustion Processes* (Nauka, Novosibirsk, 1985) [in Russian].
34. K. Hanjalić, R. van de Krol, and A. Lekic, *Sustainable Energy Technologies: Options and Prospects* (Springer, Dordrecht, London, 2008).
35. J. Janiszewski, Metrol. Meas. Syst. **19**, 797 (2012).
36. J. Janiszewski, Int. J. Sol. Struct. **49**, 1001 (2012).
37. C. del Pino, L. Parras, M. Felli, and R. Fernandez-Feria, Phys. Fluids **23**, 013602 (2011).
38. F. Corvaro, M. Paroncini, and M. Sotte, Int. J. Therm. Sci. **50**, 1629 (2011).
39. J. V. Simo Tala, S. Russeil, D. Bougeard, and J.-L. Harion, Exp. Therm. Fluid Sci. **50**, 45 (2013).
40. T. Hadad and R. Gurka, Exp. Therm. Fluid Sci. **45**, 203 (2013).
41. N. Takagaki and S. Komori, Int. J. Multiphase Flow **60**, 30 (2014).
42. L. G. Loitsanskii, *Mechanics of Gases and Liquids* (Nauka, Moscow, 1970; Pergamon, Oxford, 1975).
43. D. G. Pazhi and V. S. Galustov, *Principles of Liquid Spraying* (Khimiya, Moscow, 1984) [in Russian].
44. V. I. Terekhov and M. A. Pakhomov, *Heat Mass Transfer and Hydrodynamics in Gas–Droplet Flows* (Novosib. Gos. Tekhnol. Univ., Novosibirsk, 2009) [in Russian]

Translated by V. Smirnov